Journal of Environmental Chemical Engineering 8 (2020) 103928

Contents lists available at ScienceDirect

Journal of Environmental Chemical Engineering

journal homepage: www.elsevier.com/locate/jece

Preparation of a new adsorbent for the removal of arsenic and its simulation with artificial neural network-based adsorption models

J.A. Rodríguez-Romero[a,b], D.I. Mendoza-Castillo[b,c,*], H.E. Reynel-Ávila[b,c], D.A. de Haro-Del Rio[d], L.M. González-Rodríguez[e], A. Bonilla-Petriciolet[b], C.J. Duran-Valle[f], K.I. Camacho-Aguilar[a]

[a] Instituto Tecnológico de Tepic, Nayarit, 63175, Mexico
[b] Instituto Tecnológico de Aguascalientes, Aguascalientes, 20256, Mexico
[c] CONACYT, Cátedras Jóvenes Investigadores, 03940, Mexico
[d] Universidad Autónoma de Nuevo León, Nuevo León, 64451, Mexico
[e] Instituto Politécnico Nacional, Unidad Profesional Interdisciplinaria de Ingeniería Campus Zacatecas, Zacatecas, 98160, Mexico
[f] Universidad de Extremadura, Badajoz, 06006, Spain

ARTICLE INFO

Editor: G.L. Dotto

Keywords:
Arsenic
Artificial neural network
Adsorption modeling
Water treatment
Opuntia ficus indica

ABSTRACT

The preparation of an alternative material for the adsorption of arsenic from aqueous solution was studied. This adsorbent was obtained from the pyrolysis and $ZnCl_2$ activation of *Opuntia ficus indica* biomass (widely known as nopal), which is a typical plant of the Mexican landscape. Preparation conditions of this adsorbent were improved to increase its arsenic adsorption properties. Experimental kinetic and isotherm data for the arsenic removal with the best adsorbent were quantified to analyze its performance. A detailed physicochemical characterization of this adsorbent was carried out to obtain insights about the arsenic adsorption mechanism. A set of new isotherm and kinetic equations were also developed for modeling the arsenic adsorption. These novel models were obtained from the hybridization of the traditional adsorption equations with an artificial neural network. The artificial neural network was used to improve the performance of the conventional kinetic and isotherm equations for the simulation of arsenic removal at different conditions of pH and temperature. Performance of these models was assessed using the arsenic adsorption experimental data obtained with tested adsorbent. Results showed that hybrid models outperformed the well-known kinetic and isotherm adsorption equations commonly used in water treatment allowing better calculations for process design. These models can be extended for the study and analysis of the adsorption of a variety of water pollutants.

1. Introduction

Water pollution has become an important environmental problem of the 21 st century mainly due to the discharge of several pollutants from the industrial sector as well as from geogenic factors that contribute to alter the water quality. Arsenic is a relevant water pollutant because of its harmful effects in the human body since this metalloid can cause chronic and acute damage depending on the factors associated to its exposure route (e.g., concentration in water, exposure time) [1]. The toxicity of arsenic mainly depends of its oxidation state and the health problems caused in living organisms exposed to this metalloid include melanosis, keratosis, cancer, heart disturbance and brain damage [2,3]. In Latin America, the water pollution by arsenic affects fourteen countries including Mexico and, according to the World Health Organization [3], at least four million people have the risk to drink water with arsenic concentration higher than that established as the safe concentration threshold to prevent toxicological symptoms in the human body (i.e., 10 μg/L). Therefore, arsenic is considered as a relevant and target pollutant in the context of water treatment in several developing countries [4].

The adsorption of this geogenic pollutant has been studied and analyzed employing materials with different physicochemical properties [1,5–9]. Alternative adsorbents for the remediation of water polluted by arsenic can be prepared from wastes and by-products that are generated by agrifood industry. These precursors are attractive to prepare adsorbents for water treatment due to their low cost, diversity, renewability, biodegradability and abundance (e.g., around 1550 million of tons are generated annually) [10]. To date, carbon-based adsorbents, magnetic materials and biochars have been used to remove arsenic species from aqueous solutions [11–16]. Carbon-based

* Corresponding author.
E-mail address: didi_men@hotmail.com (D.I. Mendoza-Castillo).

https://doi.org/10.1016/j.jece.2020.103928
Received 29 January 2020; Received in revised form 31 March 2020; Accepted 31 March 2020
Available online 11 April 2020

adsorbents play an important role in water treatment since their physicochemical properties can be tailored, via the synthesis route, to remove specific pollutants [14].

Lignocellulosic biomasses are attractive precursors of carbon-based adsorbents since these feedstocks have a high content of fixed carbon, low amount of ashes and are renewable organic materials [14,17]. The main chemical constituents of these biomasses are cellulose, hemicellulose, lignin and starch [4,17]. Note that the preparation of adsorbents from these feedstocks can imply a simple process due to the high reactivity of lignocellulosic materials [14]. In fact, several lignocellulosic materials are suitable to synthetize carbon-based adsorbents [18] and the best precursors should be identified for the application at hand.

Under this context, the present study deals with the preparation of an alternative adsorbent from the pyrolysis and $ZnCl_2$ activation of *Opuntia ficus indica* biomass and its application in the arsenic removal from water. *Opuntia ficus* is a long-domesticated plant originated from arid and semi-arid regions of Mexico and it is the most widespread cactus species. It is native of South America, but it is also found in Mediterranean basin, Middle East, South Africa and India [19]. The main use of this plant is as edible fruit and cladodes production for human and animal feed. However, the dead plants could be used as adsorbents (in its raw, physically and/or chemically treated forms) for the removal of priority pollutants from water such as heavy metals, anions, pesticides and dyes [19–21]. For example, Fox et al. [22] reported the application of cactus mucilage to obtain pectic polysaccharide extracts (gelling and nongelling) from *Opuntia ficus-indica* as adsorbents of arsenic at batch conditions. Gebrekidan et al. [21] used fresh and dried *Opuntia ficus indica* pads to remove organochlorine pesticides (aldrin, dieldrin and DDT) from surface waters at batch and dynamic conditions. The fruit waste of *Opuntia ficus-indica* has been also utilized as adsorbent of textile basic (Basic Blue 9 and Basic Violet 3) and direct (Direct Green 1 and Direct Orange 26) dyes [23]. In another study, Peláez-Cid et al. [24] utilized *Opuntia ficus-indica* fruit waste to obtain three adsorbents: ashes at 550 °C, carbonized materials at 400 °C and chemically activated carbon using H_3PO_4 at 400 °C. These adsorbents were used in the removal of acid (Natural Red 4), basic (Basic Blue 9 and Basic Violet 3), direct (Direct Green 1 and Direct Turquoise 86), vat (Vat Navy Blue and Vat Dark Grey) and reactive (Reactive Blue, Reactive Red and Reactive Orange) dyes. The adsorption performance of raw and chemically treated cactus fibers for the removal of copper from water was also evaluated by Prodromou and Pashalidis [25]. Hadjittofi et al. [18] also employed cactus fibers as precursor of a carbon-based adsorbent to remove copper from aqueous solutions. The removal of hexavalent chromium from aqueous solutions with *Opuntia* cladodes and ectodermis from cactus fruits was investigated at batch conditions by Fernández-López et al. [26]. Recently, the adsorption of hexavalent uranium from aqueous solutions was also studied at batch conditions using activated biochar fibers that were obtained from *Opuntia ficus indica* [27]. Opuntia ficus-indica cactus was used to extract mucilage fractions, which were mixed with sodium alginate and calcium chloride to obtain adsorbents for arsenic removal [28]. A global analysis of the results reported in these studies has shown that this biomass is an interesting and promising precursor to prepare alternative adsorbents for water treatment.

On the other hand, it is convenient to highlight that these studies have reported the application of both traditional isotherm and kinetic equations (e.g., Langmuir, Freundlich, Sips, Pseudo-first order kinetic, Pseudo-second order kinetic) for the modeling of pollutant adsorption. These models are characterized by an analytical mathematical formulation that can be used straightforward in the adsorption data fitting. However, they may fail to fit simultaneously the adsorbent performance at different operating conditions (e.g., isotherms obtained at several temperatures or kinetics recorded at different initial concentrations) using a single set of adjustable parameters where the correlation results and predictions could be inaccurate for the adsorption process design.

In addition, the adsorption modeling of water pollutants is challenging due to this separation process involves different operating variables (e.g. pH, temperature, adsorbate concentration, adsorbent dosage) and the adsorbent performance has a nonlinear behavior. Under this scenario, the traditional adsorption equations could show limitations to simulate both kinetics and isotherms [29,30]. For example, Langmuir equation may fail for the simultaneous fitting of the experimental isotherms obtained at different conditions of pH and temperature using a single set of adjustable parameters q_{mL} and K_L. This limitation also prevails for traditional analytical kinetic equations such as the Pseudo-first or Pseudo-second order equations.

Recent studies have focused on the improvement of mathematical properties of adsorption models for process design and simulation [31]. For example, novel adsorption equations have been obtained from the application of statistical physics theory [32]. Surrogate models such as the response surface methodology or artificial neural networks have been also utilized in adsorption studies [33]. In particular, the artificial neural networks have been applied in the adsorption modeling to develop mainly empirical approaches for fitting the performance of batch and dynamic processes [33,34]. This artificial intelligence tool can be also combined with other models to develop alternative models for process design. These models can be obtained from the hybridization of adsorption equations and artificial neural networks [35,36]. A limited number of studies has been carried out to use and apply this modeling approach in the simulation of adsorption processes involved in water treatment. In fact, this type of models has been utilized only in the analysis of water defluoridation with batch and packed bed adsorbers [35,36]. In particular, two hybrid models based on artificial neural network, pseudo second order kinetic and Langmuir isotherm were proposed for fluoride adsorption. Therefore, it is convenient to develop other hybrid adsorption models and extend their application for the simulation of challenging processes such as those involved in the removal of priority water pollutants like arsenic.

Under this perspective, another objective of this paper was to introduce a set of alternative isotherm and kinetic equations that has been developed for the modeling of arsenic adsorption. These alternative adsorption models were obtained from the hybridization of the traditional adsorption equations with an artificial neural network. The artificial neural network was used to improve the performance of conventional kinetic and isotherm equations for the simulation of arsenic removal at different conditions of pH and temperature. The performance of these models was tested using the experimental data of the kinetics and isotherms for the arsenic adsorption with the adsorbent prepared from the pyrolysis and $ZnCl_2$ activation of *Opuntia ficus indica* biomass. Results showed that this alternative adsorbent was competitive for the arsenic adsorption. Also, the hybrid adsorption models outperformed the well-known kinetic and isotherm equations commonly used in water treatment allowing better calculations for process design. These models can be extended for the study and analysis of the adsorption of water pollutants.

2. Methodology

2.1. Preparation of the adsorbent and its application in arsenic removal

Adsorbents were prepared from the pyrolysis of the cladodes of *Opuntia ficus indica* (also known as nopal). This lignocellulosic biomass was obtained from Zacatecas (Mexico) and different adsorbent samples were obtained via pyrolysis. Table 1 shows the experimental design utilized to prepare the adsorbent samples. Dwell time and pyrolysis temperature were the independent variables analyzed in this experimental design. Prior to the carbonization, the precursor was impregnated with an aqueous solution of $ZnCl_2$. This solution was prepared with deionized water considering a ratio of 0.5 g of $ZnCl_2$ per gram of biomass. Precursor was soaked with this solution and further submitted to a thermal treatment at 60 °C for 24 h. This zinc-loaded

Table 1
Pyrolysis conditions for the preparation of adsorbents for arsenic removal using the *Opuntia ficus indica* biomass as precursor.

Adsorbent	Pyrolysis conditions		Yield, %	Maximum q, mg/g	pH_{pzc}
	Temperature, °C	Dwell time, h			
C400 − 2	400	2	40.70	8.17	7.42
C500 − 1	500	1	34.67	5.86	7.41
C500 − 2		2	34.13	5.49	7.39
C600 − 1	600	1	32.89	4.67	7.49
C600 − 2		2	32.15	4.31	7.32
C700 − 1	700	1	30.84	2.77	7.42
C700 − 2		2	30.36	2.53	7.37

feedstock was pyrolyzed in a tubular furnace using a load of 30 g under N_2 flow of 100 mL/min. Note that these conditions used to prepare the arsenic adsorbent from nopal biomass have not been reported in previous studies. Adsorbent yields were determined for each pyrolysis condition given in Table 1 and the adsorbent samples were washed with deionized water, dried and stored for the arsenic adsorption tests.

A preliminary screening of seven adsorbents was carried out to identify the best preparation conditions for the arsenic removal. Adsorption isotherms were obtained with these adsorbents (mean particle size of 0.67 mm) at 30 °C and pH 7. These isotherms were experimentally determined using arsenic (V) aqueous solutions with concentrations from 10 to 200 mg/L. These tests were carried out with an adsorbent dosage of 5 g/L and an equilibrium time of 24 h, which was established based on preliminary kinetic studies. Maximum adsorption capacities were estimated from these isotherms and the best adsorbent for arsenic removal was identified. The thermodynamic adsorption behavior of the best adsorbent was characterized via additional kinetic and equilibrium studies at different conditions of temperature (i.e., 30 and 40 °C) and pH (i.e., 6 and 7) employing arsenic (V) solutions with initial concentrations from 10 to 200 mg/L. Arsenic adsorption enthalpy was calculated with the partition coefficient for diluted solutions obtained from the isotherms and Van't Hoff's approach.

All adsorption experiments were done by duplicate and the adsorbate quantification in the aqueous solutions was carried out with atomic absorption spectroscopy using an iCE 3300 Thermo Scientific equipment. Mean values of the replicates were utilized in data analysis and the arsenic adsorption capacities (q, mg/g) were calculated employing a mass balance

$$q = \frac{V([As]_0 - [As]_t)}{m_{char}} \quad (1)$$

where m_{char}/V (g/L) is the dosage of adsorbent to adsorbate solution used in the removal tests, $[As]_0$ and $[As]_t$ are the initial and final arsenic concentrations quantified in the adsorption experiment (mg/L).

Textural parameters of adsorbent samples were determined via N_2 adsorption/desorption isotherms, while the pH at the point of zero charge (p.z.c.) was estimated following the methodology reported in other studies [37]. FTIR spectra of adsorbents with and without loaded arsenic were recorded with a Nicolet iS10 Thermo Scientific spectrometer. These spectra were obtained with 32 scans per sample in the range of 4000 to 400 cm^{-1} and a resolution of 4 cm^{-1} where the adsorbents were previously mixed with KBr (reactive grade) to be measured as pellets. X-ray diffraction (XRD) analyses of precursor and adsorbents were done using an Empyrean (Malvern-PANalytical) diffractometer equipped with a PIXcel 1D detector at 40 mA and 45 kV of current and electrical voltage. XRD measurements were performed in powder setting mode using zero background silicon single crystal substrates holders and CuK_α radiation (λ = 1.5406 Å). XRD data were collected at room temperature in the Bragg-Brentano reflection geometry, at a scattering angle from 10 to 150° (2θ), step size of 0.0263° (2θ) and scan step time of 147 s. The incident beam pathway included a 0.04 rad soller slit, 0.125° fixed divergence slit and, 0.5° anti-scattering slit, while a 0.04 rad soller slit and anti-scatter slit (7.5 mm) were used in the diffracted beam optic. HighScore Plus software and the structural PDF-2 database were utilized to identify the crystalline phases in the samples. Organic elemental composition of adsorbents was quantified with a LECO CHNS 932 equipment where the oxygen content was estimated by difference. Wavelength dispersive X-ray fluorescence (WDXRF) analysis was done with a Bruker S8 Tiger spectrometer, while the adsorbent morphology was observed via SEM/EDX with a FEI Quanta 3D FEG equipment.

2.2. Description of hybrid models for the arsenic adsorption using an artificial neural network

A set of alternative models for the arsenic adsorption has been developed considering the hybridization of analytical isotherm and kinetic equations with an artificial neural network. The application of a hybrid approach to improve the fitting properties of two adsorption models for fluoride removal has been already described [35]. This study was the first step to develop alternative equations that can be used for the analysis of the adsorption processes involved in water pollution control. Therefore, other adsorption hybrid models are introduced in this paper for analyzing the arsenic removal from aqueous solution at batch conditions. They are based on the hybridization of several well-known analytical adsorption equations and a feed-forward artificial neural network. In these hybrid models, the neural network was used to estimate the parameters of kinetic and isotherm equations as a function of the independent variables involved in the adsorption process. For example, Fig. 1 illustrates this approach for both kinetic and isotherm models. This hybridization increased the capabilities of adsorption model for fitting and predicting the adsorbent performance at different operating scenarios.

Overall, the independent variables involved in the kinetic experiments for arsenic adsorption were the initial adsorbate concentration $[As]_0$, temperature T, pH and time t, while the experimental isotherms comprised the equilibrium adsorbate concentration $[As]_e$, T and pH. The arsenic adsorption capacity q was the dependent variable for both cases. Note that the operating parameters of the adsorption process (e.g., pH, temperature, initial adsorbate concentration) have been used as input variables in other studies reported in the literature for adsorption modeling with artificial neural networks [35,36,38]. Therefore, it has been assumed that the adsorption model parameters θ_i have nonlinear relationships with these independent variables. These relationships can be defined as $\theta_1,\ldots,\theta_{npar} = f([As]_0, T, pH, t)$ for kinetics and $\theta_1,\ldots,\theta_{npar} = f([As]_e, T, pH)$ for isotherms. Then, a feed-forward artificial neural network was used to establish these relationships. For the case of the arsenic adsorption kinetics, the hybrid model is given by

$$z_{1j} = \frac{T}{T_{max}} w_{1j1} + \frac{pH}{pH_{max}} w_{1j2} + \frac{t}{t_{max}} w_{1j3} + \frac{[As]_0}{[As]_{0,max}} w_{1j4} + b_{1j}\, j = 1,\ \ldots, n_{hid} \quad (2)$$

$$y_{1j} = f_{ANNs}(z_{1j})\, j = 1,\ \ldots, n_{hid} \quad (3)$$

$$\theta_i = \sum_{k=1}^{n_{hid}} (y_{1k} w_{2ik}) + b_{2i}\, i = 1,\ \ldots, n_{par} \quad (4)$$

$$q_t = f_{Kin}(\theta_1, \ldots, \theta_{n_{par}}) \quad (5)$$

where f_{ANNs} is the activation function of the artificial neural network, w is a weight factor, b is a bias parameter, n_{hid} is the number of hidden neurons (i.e., processing units) of the neural network and f_{Kin} is the kinetic functionality used in the calculations. Eqs. (2) and (5) are replaced by Eqs. (6) and (7) for the analysis of arsenic adsorption isotherms

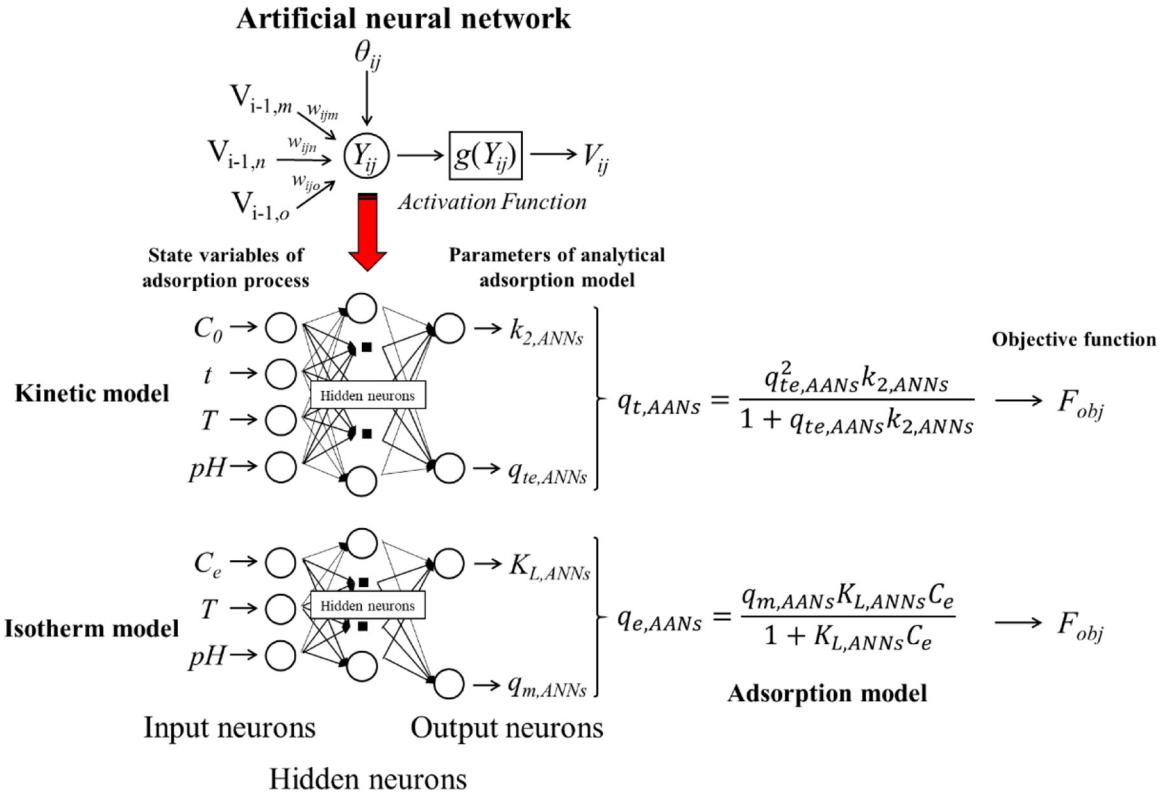

Fig. 1. Illustration of the incorporation of an artificial neural network to determine the parameters of adsorption kinetic and isotherm models.

$$z_{1j} = \frac{T}{T_{max}} w_{1j1} + \frac{pH}{pH_{max}} w_{1j2} + \frac{[As]_e}{[As]_{e,max}} w_{1j3} + b_{1j}\, j = 1,\ ..., n_{hid} \tag{6}$$

$$q_e = f_{Iso}(\theta_1,\ ..., \theta_{n_{par}}) \tag{7}$$

where f_{Iso} is the respective functionality employed to describe the adsorption equilibrium.

Functionalities f_{Kin} and f_{Iso} corresponded to the traditional adsorption equations used for kinetic and isotherm modeling. Table S1 of Supplementary Material shows the functionalities assessed to calculate the arsenic adsorption from aqueous solution. Note that several kinetic and isotherm functionalities have been analyzed where all kinetic models implied two parameters, while isotherms equations with two and three parameters were studied. Then, the artificial neural network was responsible of estimating the parameters of these equations to provide the best fit of experimental arsenic adsorption data. Activation function f_{ANNs} was also a relevant issue to improve the capabilities of tested hybrid adsorption models. Preliminary calculations were done with different activation functions for the modeling of arsenic adsorption kinetics and isotherms and the results showed that the best activation function was

$$f_{ANN} = \frac{1}{1 + exp^{-z_{1j}}} \tag{8}$$

The set of hybrid kinetic and isotherm models was labeled as ANNs-*type* where *type* corresponded to the adsorption equation. For example, ANNs-Freundlich model was the hybrid isotherm obtained from the Freundlich-type functionality with the feed-forward artificial neural network using the activation function given by Eq. (8).

Parameter estimation for these hybrid adsorption models was focused on the determination of the values of *w* and *b*. A nonlinear regression was employed to calculate these parameters via the global minimization of the next objective function F_{obj}

$$F_{obj} = \sum_{i=1}^{n_{dat}} \left(\frac{q_i^{exp} - q_i^{mod}}{q_i^{exp}} \right)^2 \tag{9}$$

where q^{exp} is the experimental arsenic adsorption capacity, q^{mod} is the calculated value of this adsorption capacity with tested adsorption model and n_{dat} is the number of experimental data included in the nonlinear regression. The minimization of Eq. (9) was done with the Simulated Annealing optimizer. The comparison between hybrid models and analytical adsorption equations was performed based on the results of final value of objective function, mean modeling error (*E*, %) and determination coefficients (R^2 and R^2_{adj})

$$E = \frac{100}{n_{dat}} \sum_{i=1}^{n_{dat}} \left| \frac{q_i^{exp} - q_i^{mod}}{q_i^{exp}} \right| \tag{10}$$

$$R^2_{adj} = 1 - (1 - R^2)\left(\frac{n_{dat} - 1}{n_{dat} - n_{adj}} \right) \tag{11}$$

where n_{adj} is the number of adjustable parameters of the adsorption model. Note that $n_{adj} = n_{par}$ for the analytical adsorption models, while n_{adj} comprised the set of *w* and *b* of the artificial neural network used to calculate θ_i in the hybrid ANNs adsorption model. Data modeling was performed with 27 and 54 experimental points from isotherms and kinetics where 80 % was utilized for ANNs training, 10 % for validation and 10 % for testing. These adsorption data showed an experimental error lower than 5%.

3. Results and discussion

3.1. Preparation of the adsorbent and its arsenic adsorption kinetics and isotherms

Table 1 reports the yields of adsorbents obtained from the *Opuntia ficus indica* biomass. These yields ranged from 30.4 to 40.7 % and they depended on the pyrolysis temperature and dwell time. Adsorbent

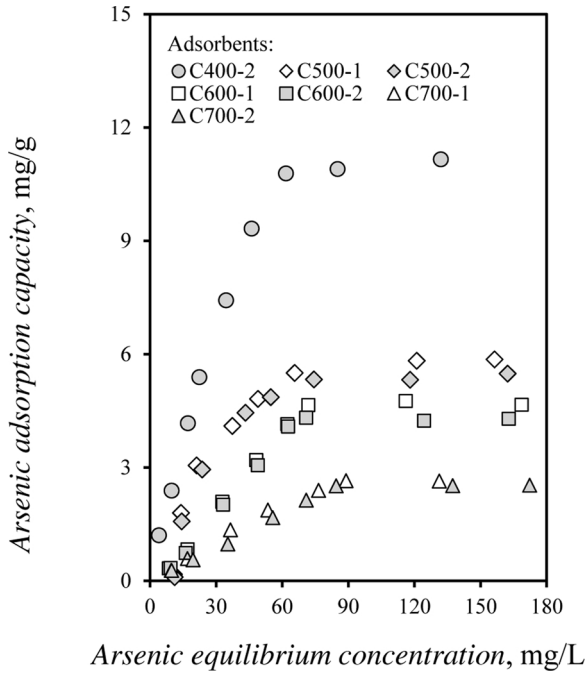

Fig. 2. Arsenic adsorption isotherms of the adsorbents obtained from *Opuntia ficus indica* biomass. Removal conditions: 30 °C and pH 7.

yields decreased with increments on these operating variables of pyrolysis, which has been recognized as a typical trend for the preparation of adsorbents obtained from lignocellulosic biomasses impregnated with $ZnCl_2$ and carbonized [39]. The arsenic adsorption isotherms of the adsorbents obtained at different pyrolysis conditions are reported in Fig. 2 where the maximum adsorption capacities are also given in Table 1. These isotherms indicated that the maximum adsorption of arsenic ranged from 2.53 to 8.17 mg/g at 30 °C and pH 7. These adsorption capacities are competitive with respect to other arsenic adsorbents reported in the literature [4–7,11,12,15,22,37,50], which may range from 0.03 to 30.48 mg/g.

Overall, the adsorbents prepared with the highest pyrolysis temperature and dwell time showed the lowest arsenic adsorption ~ 2.53 mg/g. Pyrolysis temperature affected significantly the arsenic adsorption properties of these samples where 400 °C was the best condition to prepare the adsorbent. The increment of dwell time also reduced the arsenic adsorption capacities of adsorbents but its effect was lower than that obtained for the pyrolysis temperature, see Fig. 2 and Table 1. In fact, the pyrolysis temperature used to obtain the adsorbents was the most important variable due to its impact on both textural parameters and surface chemistry. BET surface area of adsorbents increased with the pyrolysis temperature and ranged from 43.5 to 269.6 m^2/g, see Table 2. Note that a significant improvement (i.e., up to 468 %) in the surface area was obtained at the highest pyrolysis temperature (i.e., 700 °C) but the arsenic adsorption capacities of these adsorbents

Table 2
Textural parameters and organic elemental composition of selected adsorbents used in the arsenic adsorption.

Adsorbent	S_{BET}, m^2/g	V_{micro}, cm^3/g	r_p, nm	E_{ads}, kJ/mol	Ultimate analysis, %			
					C	H	N	O
C400 – 2	47.47	0.006	1.65	7.90	47.70	3.26	1.13	27.15
C500 – 2	43.54	0.007	1.29	10.11	53.40	2.40	1.06	24.52
C600 – 2	238.72	0.107	0.63	20.69	55.70	2.21	0.92	21.11
C700 – 2	269.60	0.122	0.60	21.52	56.80	1.27	0.63	25.08

decreased. The micropore volume ranged from 0.006 to 0.122 cm^3/g where adsorbents C600 – 2 and C700 – 2 showed the highest values. The mean pore radius varied from 0.604 to 1.646 nm, which also decreased with respect to the temperature utilized in the adsorbent preparation. Calculated N_2 adsorption energies for these adsorbents varied from 7.9 to 21.5 kJ/mol.

On the other hand, SEM images of adsorbent samples are reported in Fig. S1 of Supplementary Material. All adsorbents showed a highly developed porous structure with a tunnel-shape and honeycomb-like morphology. The organic elemental composition of selected adsorbents is also reported in Table 2. C content in the adsorbents increased from 47.7 to 56.8 % when the pyrolysis temperature varied from 400 to 700 °C, while the content of N and O showed the opposite trend. SEM/EDX and WDXRF analyses confirmed the presence of zinc in all adsorbents (15.22–20.18 mass %), which was consistent with the $ZnCl_2$ chemical activation of the biomass before its pyrolysis. Calcium, magnesium and aluminum were also identified in the adsorbent samples but in trace levels. It is interesting to observe that the adsorbent with the highest amount of zinc (i.e., C400 – 2) showed the best arsenic removal and the lowest surface area. These results contributed to conclude that the adsorbent surface chemistry played a fundamental role for the arsenic adsorption. Previous studies have reported that activated carbons and adsorbents containing metallic oxides were effective for arsenic adsorption [37,40]. The presence of the metal oxides on the adsorbent surface could interact with arsenic forming metal–arsenic compounds [40]. Therefore, it could be expected that these interactions were present in the arsenic adsorption mechanism. The values of p.z.c. of all adsorbents ranged from 7.32 to 7.49 indicating that they showed a positively charged surface at pH 7 that also promoted the adsorption of arsenic species (i.e., $HAsO_4^{-2}$ and H_2AsO_4-) at pH ≤ 7 via attractive electrostatic forces.

Fig. S2 of Supplementary Material shows the maximum arsenic adsorption capacities of all adsorbents at pH conditions from 6 to 8. Arsenic removal decreased with increments on solution pH and the maximum adsorption was obtained at pH 6. Adsorption capacities ranged from 4.23 to 8.32 mg/g at pH 6, 2.14–7.43 mg/g at pH 7 and 0.76–6.12 mg/g at pH 8, respectively. These adsorption capacities decreased up to 49 % from pH 6–7 and 70 % from pH 7–8, see Fig. S2. This decrement in the adsorption capacities was due to the changes on the adsorbent surface charge, which passed from positive to negative due to the increment of pH causing electrostatic repulsive forces between the arsenic anions and the adsorbent surface because pH > p.z.c. Also, the presence of OH^- ions in aqueous solution increased with pH changes generating a competitive effect for the binding sites of the adsorbent. The impact of pH on arsenic adsorption performance was more significant for adsorbents obtained at 700 °C, while the sample C400 – 2 prepared at 400 °C and 2 h of pyrolysis showed the best removal at all pH conditions.

FTIR results showed that the adsorbent C400 – 2 contained several functional groups, see Fig. 3. The characteristic absorption bands associated to the adsorbents prepared from lignocellulosic biomasses were identified in the infrared spectra given in Fig. 3. Specifically, the O—H stretching vibration was observed at 3420 cm^{-1}, while the absorption bands of the stretching and bending vibrations of aliphatic C–H bonds were identified between 2920 – 2850 and 1450 – 1200 cm^{-1}, respectively [41]. C—O vibration at 1620 cm^{-1} can be related to carboxylic, ester or aldehyde groups [42]. The signal observed at 1050 cm^{-1} can be assigned to C—O stretching and Zn-O-H bending vibrations of a mixture of primary, secondary and tertiary alcohols, esters and ethers [43]. Some changes in the FTIR spectra were identified for the adsorbents obtained at higher pyrolysis temperatures especially for the absorption bands associated to oxygen-containing functionalities like carboxylic, ester and aldehyde. The changes observed in these organic functional groups could be explained as a decomposition of lignocellulosic structure during the pyrolysis that diminished and/or contributed to their exposing [44]. Note that the

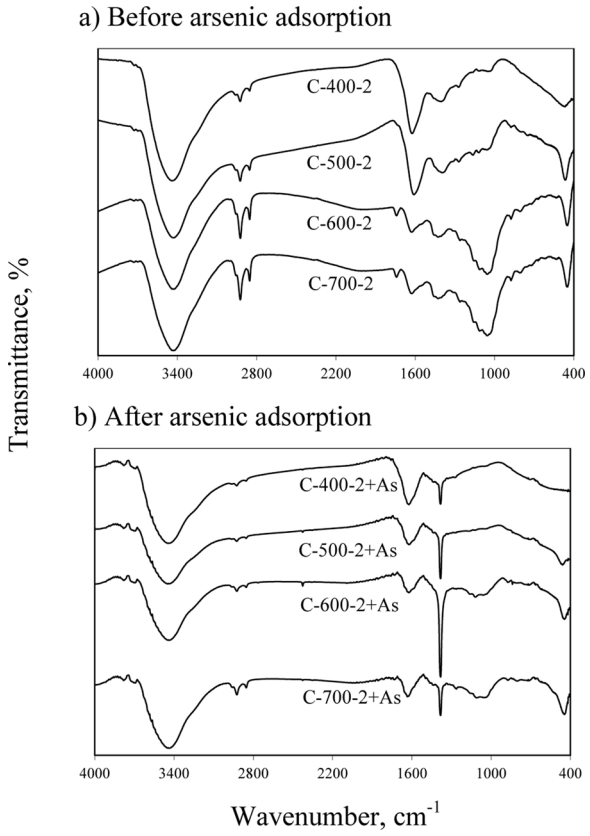

Fig. 3. FTIR spectra of adsorbents obtained from *Opuntia ficus indica* biomass.

absorption bands observed at 880 and 450 cm^{-1} corresponded to the stretching vibrations of Zn − OH and Zn-O, respectively [43]. Fig. 3b shows that a new absorption band appeared at ~1390 cm^{-1} after arsenic adsorption, which can be associated to the formation of metal-arsenate bonds [45]. Absorption bands located at 3420, 1740, 1620, 1050, 880 and 450 cm^{-1} decreased and slightly shifted providing an evidence of the role of these functionalities in the arsenic binding on the adsorbent surface [1]. Similar findings have been reported for the removal of arsenic with different adsorbents [9]. It has been suggested that the arsenic adsorption could imply the formation of a surface complex metal-O-As via the ligand exchange of hydroxyl group with arsenic species.

Fig. 4 reports the XRD patterns of analyzed samples of *Opuntia ficus indica* precursor and adsorbents. Raw and $ZnCl_2$ impregnated biomass showed diffraction peaks at ~16, 22 and 34° (2θ) that are characteristic of cellulose I_β lattice [46]. The only difference between these two samples was the crystallinity, which decreased after the pretreatment with $ZnCl_2$. This effect could be ascribed to the softening of lignocellulosic structure since $ZnCl_2$ solution swelled the natural polymers contained in the precursor [47]. After the biomass pyrolysis, the crystalline peaks of these polymers disappeared due to the formation of a graphitic structure that contained zinc oxide. The graphitic structure exhibited its typical broad diffraction peak at ~25° (2θ) that was an indicative of the stacking of a few graphene–like layers into the carbon-based adsorbent [14]. According with Hong et al. [48], the presence of ZnO onto the adsorbent surface resulted from the next reactions associated to the chemical activation

$$ZnCl_2 + H_2O \rightarrow H[ZnCl_2(OH)] \quad (12)$$

$$H[ZnCl_2(OH)] \xrightarrow{\Delta} ZnO + 2HCl \quad (13)$$

It was observed that the XRD peaks became narrower indicating a gradual increment of the crystallinity of adsorbents obtained at high temperatures. It could be expected that pyrolysis temperature promoted the degradation of natural polymer molecules, the recrystallization of some carbon material in the adsorbent and the structural orderliness within the residual solid matrix [49]. After the arsenic adsorption, a reduction in the crystalline structure of all adsorbents was observed and two new DRX peaks were detected at ~29 and 39° (2θ) that corresponded to arsenic species. These results indicated that the ZnO could act as an adsorption site for the arsenic removal. The graphitic structure of the adsorbent also played a relevant role in the arsenic adsorption since it was inversely proportional to the increment in the adsorbent crystallinity. In summary, these characterization results supported the role of −OH groups and Zn moieties on the arsenic adsorption, which were consistent with the findings from different studies [9,37,50].

Arsenic adsorption kinetics obtained with the best adsorbent C400 − 2 at different conditions of pH and temperature are given in Fig. 5a-c, while the adsorption isotherms are reported in Fig. 5d. Arsenic adsorption capacities ranged from 0.89 to 12.81 mg/g at tested operating conditions. Both kinetics and isotherms showed the presence of an endothermic arsenic adsorption and, also confirmed the trend of pH on adsorbent performance where the adsorption capacities decreased with pH increments. Adsorption enthalpy was 68.4 kJ/mol suggesting that both physical and chemical interactions could be involved in the removal of arsenic using this adsorbent. Finally, this set of experimental data were used to validate and compare the adsorption models proposed in the present manuscript.

3.2. Application of hybrid isotherm and kinetic models for the arsenic adsorption

Results of the adsorption kinetic and isotherm modeling are reported in Table 3 and Fig. 6. Two hidden neurons were used for the calculations with the artificial neural network in the hybrid models. First, a comparison of the adsorption models was performed with their corresponding counterparts. Table 3 and Fig. 6 showed that all traditional kinetic and isotherm equations were outperformed by the ANNs-based adsorption models. The mean modeling errors of analytical kinetic equations ranged from 7.11 to 35.39 % with R^2_{adj} from 0.32 to 0.98 where the Pseudo-second order kinetic was the best option. First order kinetic equation failed to obtain a proper data fitting of arsenic adsorption data (R^2_{adj} = 0.32). Therefore, the model performance of these kinetic equations was: Pseudo-second order > Pseudo-first order > First order. On the other hand, the hybrid kinetic models showed the lowest mean modeling errors (i.e., from 4.97 to 7.64 %) and the highest R^2_{adj} values (i.e., from 0.95 to 0.99). All ANNs-based models fitted satisfactorily the arsenic adsorption kinetics where the numerical performance was: ANNs-Pseudo-second order > ANNs-Pseudo-first order ≅ ANNs-First order. Herein, it is convenient to remark that the parameters of all kinetic analytical equations were determined via the data fitting of a specific set of experimental data (i.e., adsorption kinetic obtained for constant state variables: pH, temperature and initial adsorbate concentration), while the parameters of hybrid ANNs models were obtained from the simultaneous regression of all experimental kinetics. This implied that the parameters of conventional adsorption models were constant for a given set of experimental conditions, while the parameters of hybrid adsorption models are regarded as nonlinear functionalities of the input variables utilized to train the artificial neural network thus improving their flexibility and data correlation capabilities. These results clearly proved that the incorporation of the ANNs to estimate the parameters of tested analytical kinetic equations improved significantly the modeling results. The best example to illustrate this improvement is the ANNs-First order model, which offered a satisfactory correlation of the arsenic adsorption kinetics in contrast to the corresponding non-hybrid kinetic equation.

The analytical isotherm equations were also outperformed by the equivalent hybrid ANNs models. Modeling errors of these analytical equations were 7.17–20.13 %, which were higher than those obtained

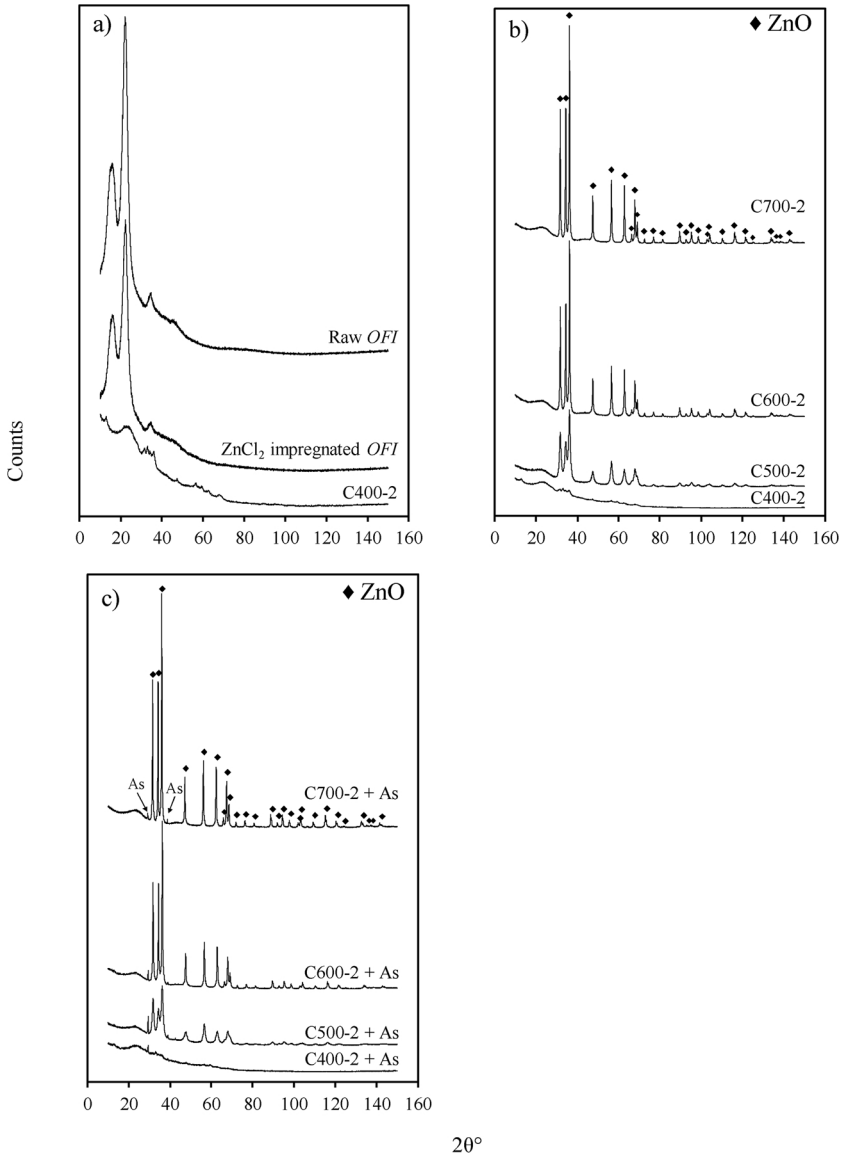

Fig. 4. X-ray diffraction analysis for the precursor and adsorbents obtained for the adsorption of arsenic from aqueous solution. OFI corresponds to the *Opuntia ficus indica* biomass; C400-2, C500-2, C600-2 and C700-2 are the adsorbents obtained with preparation conditions given in Table 1. Symbol As indicates the presence of arsenic on the adsorbent.

with the hybrid ANNs isotherm models (i.e., 2.22–2.90 %). Freundlich equation showed the worst fitting with $R^2_{adj} = 0.80$ and remaining analytical equations showed a similar performance for the correlation of arsenic adsorption isotherms although some models have three adjustable parameters. Note that the Redlich-Peterson, Langmuir-Freundlich and Toth isotherms can approach the performance of Langmuir equation if the adjustable parameters B_{RP}, n_T and $n_{LF} \rightarrow 1$ [29]. The results of the parameter estimation of these models satisfied this condition with tested experimental data and, consequently, these isotherm equations displayed the same modeling behavior. On the other hand, all hybrid ANNs isotherms showed $R^2_{adj} \geq 0.98$ with low mean modeling errors (< 3 %), see Table 3. The performance of ANNs-Redlich-Peterson, ANNs-Langmuir-Freundlich and ANNs-Toth models was slightly better than those of ANNs-Freundlich and ANNs-Langmuir. In particular, ANNs-Langmuir-Freundlich model was selected as the best option to model the adsorption arsenic because it was less sensitive to the overfitting.

For illustration, a detailed error analysis of all kinetic and adsorption models as a function of the adsorption conditions is provided in Fig. 6. These results corroborated that First order kinetic and Freundlich isotherm equations displayed the highest modeling errors at tested experimental adsorption conditions. Figs. S3 – S5 of Supplementary Material indicated that these analytical equations provided several outliers due to the underestimations of the arsenic adsorption capacities. The misfit of both models can be corrected significantly using ANNs. Overall, the under- or over-estimations of output models were reduced for both kinetics and isotherms with the proposed hybrid calculation approach. The accuracy of these ANNs-based adsorption models can be improved if the number of hidden neurons is increased. For instance, the mean modeling error and R^2_{adj} of ANNs-First order model were 2.39 % and 0.9938 using 3 hidden neurons, which were better than those reported for this model but with 2 hidden neurons, see Table 3. Same trends were obtained for remaining hybrid adsorption models. Under this scenario, it is necessary to identify a proper tradeoff of the model structure to avoid the adsorption data overfitting.

As stated, parameters of the hybrid ANNs adsorption models depended on the state variables of both kinetics and isotherms where Fig. 7 illustrates this behavior. For example, the adjusted parameters of the conventional Pseudo-second order model were $q_{tep2} = 5.98$ mg/g and $k_{p2} = 0.21$ g/mg h at pH 7, 40 °C and 40 mg/L, while the

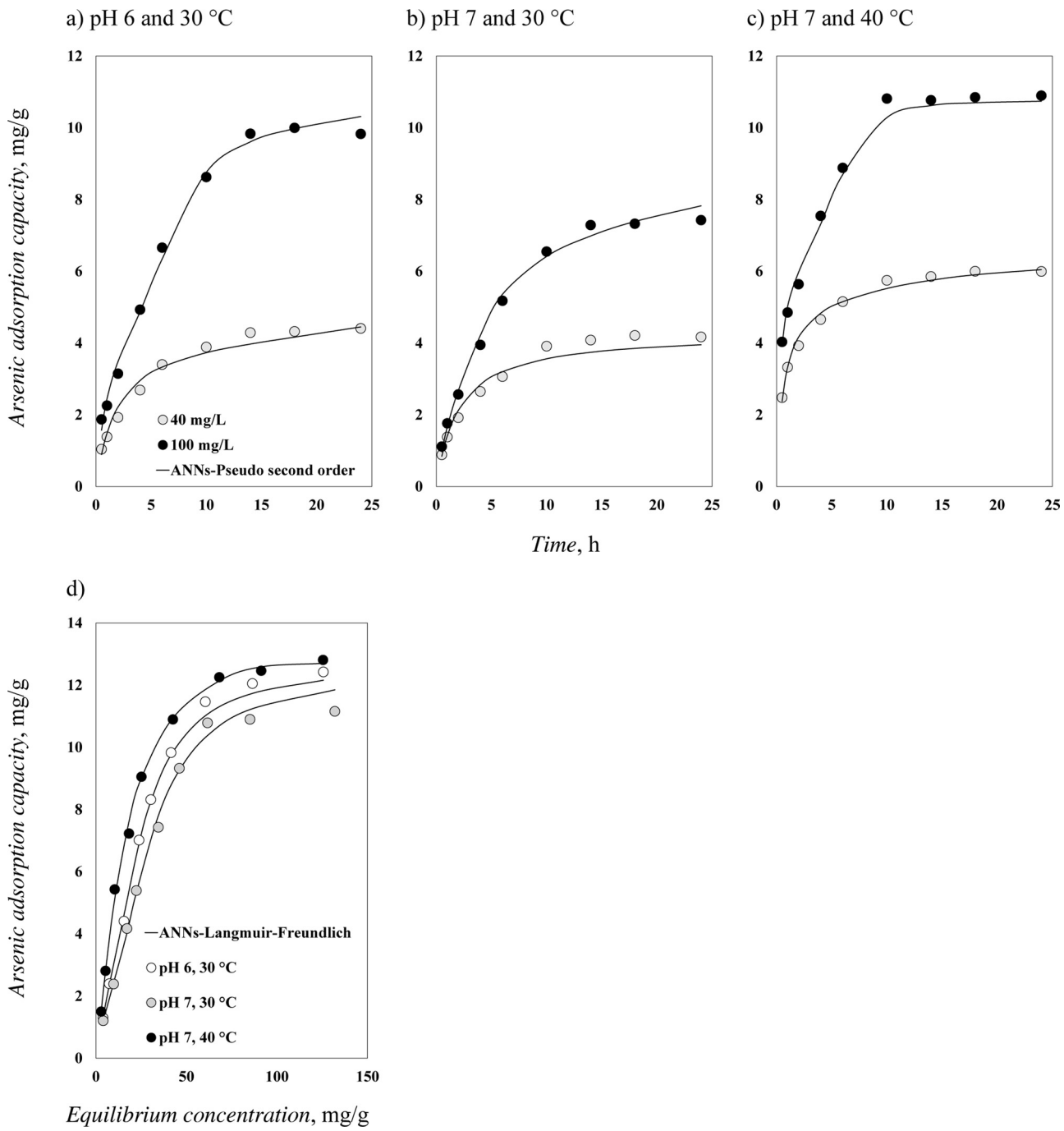

Fig. 5. a,b,c) Arsenic adsorption kinetics and d) isotherms in aqueous solution using adsorbent C400-2.

parameters of ANNs-Pseudo-second order model ranged from 5.27 to 6.13 mg/g for $q_{tep2,ANNs}$ and from 0.31 to 0.49 g/mg h for $k_{p2,ANNs}$, respectively. Note that similar results were obtained for all adsorption models. Therefore, the parameter values of the adsorption functionality used in the modeling were adapted via the artificial neural network to improve the quality of data fitting of kinetics and isotherms. This feature allowed the flexibility of model to fit, with a high accuracy, the adsorption data obtained at different operating conditions.

4. Conclusions

An alternative adsorbent for the arsenic removal was prepared from the pyrolysis and $ZnCl_2$ activation of a typical mexican biomass. The preparation route of this adsorbent was improved to increase its arsenic adsorption properties. Arsenic adsorption mechanism could imply surface complexes of metal-O-As where a ligand exchange of hydroxyl group with arsenic species occurred. Alternative hybrid adsorption models have been also introduced and applied for the analysis of arsenic removal from aqueous solutions. These models were obtained by the hybridization of an artificial neural network and analytical kinetic and isotherms equations. Results showed that these hybrid models outperformed the analytical equations widely applied in the adsorption modeling of water pollutants. The integration of the artificial neural network for the parameter identification of adsorption models allowed flexibility for the simultaneous fitting of experimental data obtained at different operating conditions. These models can be utilized to fit the experimental adsorption data of others water pollutants and adsorbents, and for calculations involved in the process design of water

Table 3
Results of the arsenic adsorption simulation with the analytical equations and hybrid ANNs-based models.

Model	F_{obj}	Modeling error, %	R^2	R^2_{adj}
First order	8.59	35.39	0.3174	0.3043
Pseudo-first order	1.05	11.32	0.9532	0.9523
Pseudo-second order	0.50	7.11	0.9781	0.9777
ANNs-First order	0.50	7.64	0.9632	0.9487
ANNs-Pseudo-first order	0.38	6.60	0.9652	0.9515
ANNs-Pseudo-second order	0.22	4.97	0.9939	0.9915
Langmuir	0.19	7.17	0.9669	0.9656
Freundlich	1.57	20.13	0.8076	0.7999
Redlich-Peterson	0.19	7.17	0.9669	0.9641
Langmuir-Freundlich	0.19	7.17	0.9669	0.9641
Toth	0.19	7.17	0.9669	0.9641
ANNs-Langmuir	0.03	2.90	0.9943	0.9886
ANNs-Freundlich	0.03	2.61	0.9945	0.9890
ANNs-Redlich-Peterson	0.03	2.33	0.9957	0.9888
ANNs-Langmuir-Freundlich	0.02	2.22	0.9960	0.9896
ANNs-Toth	0.03	2.54	0.9973	0.9929

treatment technologies.

CRediT authorship contribution statement

J.A. Rodríguez-Romero: Methodology, Investigation. **D.I. Mendoza-Castillo:** Formal analysis, Investigation, Writing - review & editing. **H.E. Reynel-Ávila:** Investigation, Writing - review & editing. **D.A. de Haro-Del Rio:** Investigation, Writing - review & editing. **L.M. González-Rodríguez:** Investigation, Writing - review & editing. **A. Bonilla-Petriciolet:** Software, Supervision, Project administration, Writing - review & editing. **C.J. Duran-Valle:** Formal analysis, Investigation, Writing - review & editing. **K.I. Camacho-Aguilar:** Writing - review & editing.

Declaration of Competing Interest

The authors declare that they have no known competing financial interests or personal relationships that could have appeared to influence the work reported in this paper.

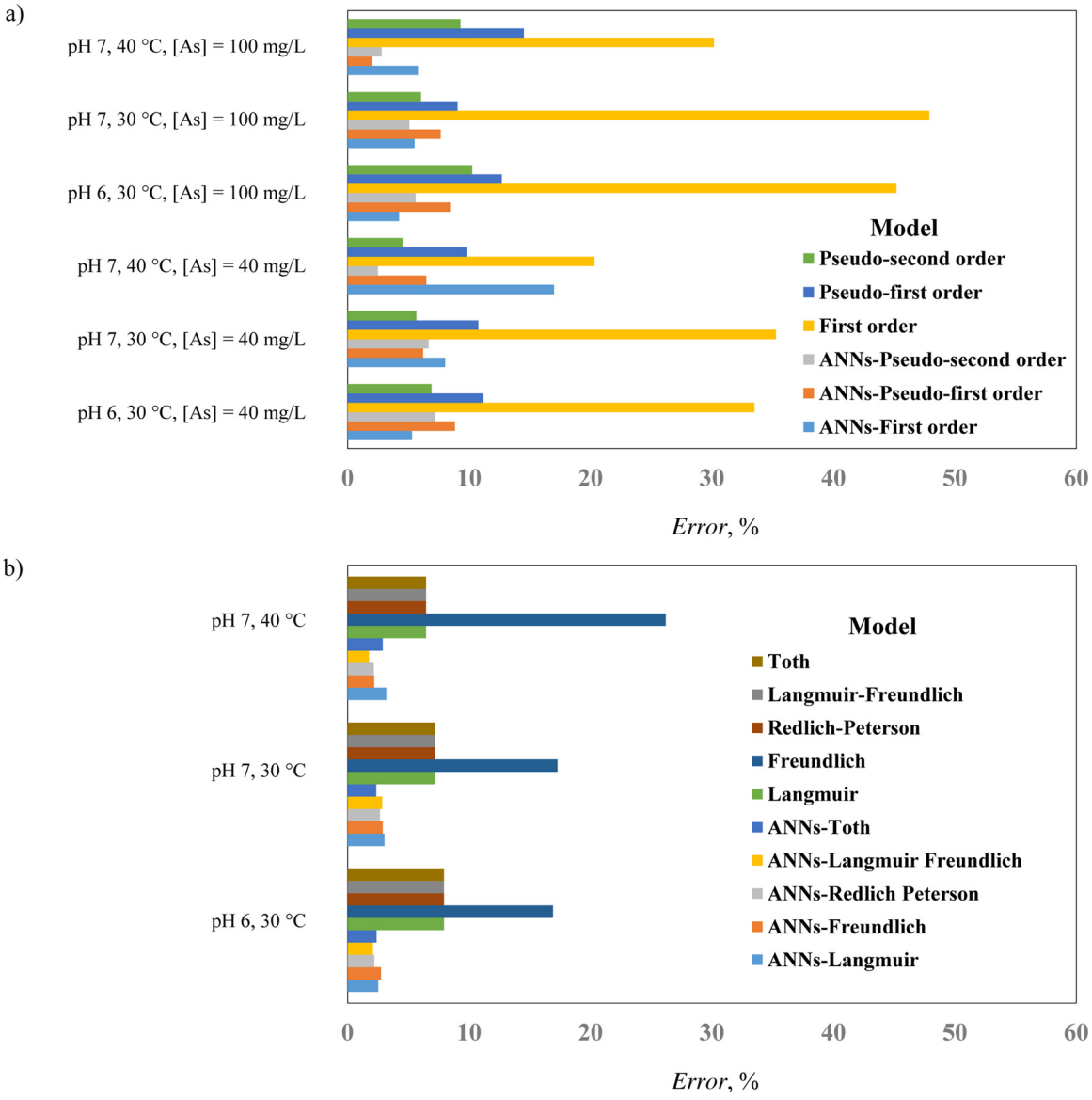

Fig. 6. Results of tested adsorption models for the arsenic adsorption on adsorbent C400-2 at different conditions of pH and temperature.

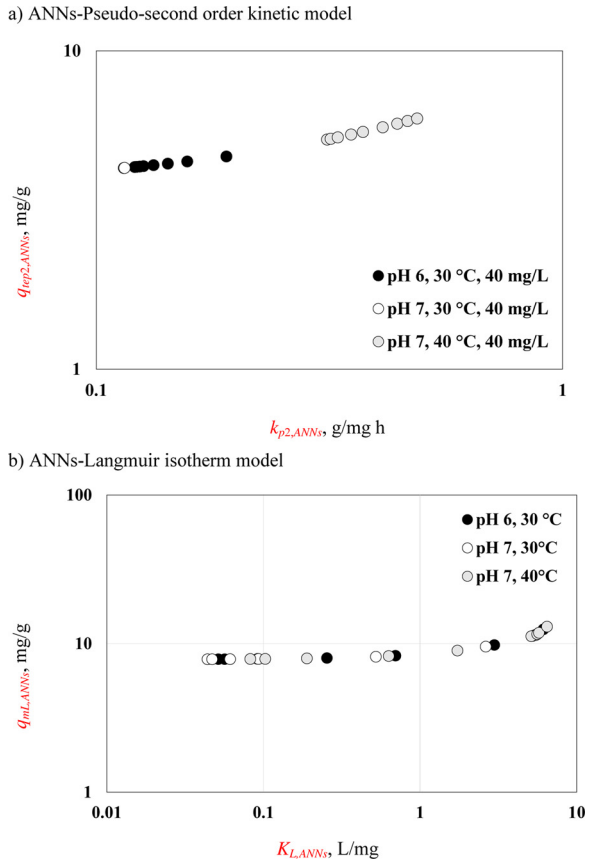

Fig. 7. Parameters of ANNs-Pseudo-second order kinetic and ANNs-Langmuir isotherm models for the calculation of the arsenic adsorption using adsorbent C400-2.

Appendix A. Supplementary data

Supplementary material related to this article can be found, in the online version, at doi:https://doi.org/10.1016/j.jece.2020.103928.

References

[1] K. Zhang, D. Zhang, K. Zhang, Arsenic removal from water using a novel amorphous adsorbent developed from coal fly ash, Water Sci. Technol. 73 (2016) 1954–1962, https://doi.org/10.2166/wst.2016.028.

[2] S. Shankar, U. Shanker, Shikha, Arsenic contamination of groundwater: a review of sources, prevalence, health risks, and strategies for mitigation, Sci. World J. (2014), https://doi.org/10.1155/2014/304524.

[3] WHO, World Health Organization, Arsenic, (2018) https://www.who.int/news-room/fact-sheets/detail/arsenic.

[4] R. Singh, S. Singh, P. Parihar, V.P. Singh, S.M. Prasad, Arsenic contamination, consequences and remediation techniques: a review, Ecotox. Environ. Safe. 122 (2015) 247–270, https://doi.org/10.1016/j.ecoenv.2014.10.009.

[5] M.M. Islam, A. Adak, P.K. Paul, Characterization of sweetmeat waste and its suitability for sorption of As(III) in aqueous media, Water Environ. Res. 89 (2017) 312–322, https://doi.org/10.2175/106143016X14609975747810.

[6] D. Mohan, C.U. Pittman, Arsenic removal from water/wastewater using adsorbents – a critical review, J. Hazard. Mater. 142 (2007) 1–53, https://doi.org/10.1016/j.jhazmat.2007.01.006.

[7] B. Te, B. Wichitsathian, C. Yossapol, W. Wonglertarak, Development of low-cost iron mixed porous pellet adsorbent by mixture design approach and its application for arsenate and arsenite adsorption from water, Adsorp. Sci. Technol. 36 (2018) 372–392, https://doi.org/10.1177/0263617417693626.

[8] V.B. Yadav, R. Gadi, S. Kalra, Clay based nanocomposites for removal of heavy metals from water: a review, J. Environ. Manage. 232 (2019) 803–817, https://doi.org/10.1016/j.jenvman.2018.11.120.

[9] L. Zhang, T. Zhu, X. Liu, W. Zhang, Simultaneous oxidation and adsorption of As(III) from water by cerium modified chitosan ultrafine nanobiosorbent, J. Hazard. Mater. 308 (2016) 1–10, https://doi.org/10.1016/j.jhazmat.2016.01.015.

[10] D.I. Mendoza-Castillo, H.E. Reynel-Ávila, A. Bonilla-Petriciolet, C. Pastore, L. di Bitonto, Avocado seeds valorization as adsorbents of priority pollutants from water, Bulg. Chem. Commun. 51 (B) (2019) 124–127, https://doi.org/10.34049/bcc.51.B.009.

[11] T.S. Anirudhan, M.R. Unnithan, Arsenic (V) removal from aqueous solutions using an anion exchanger derived from coconut coir pith and its recovery, Chemosphere 66 (2007) 60–66, https://doi.org/10.1016/j.chemosphere.2006.05.031.

[12] Y. Tian, M. Wu, X. Lin, P. Huang, Y. Huang, Synthesis of magnetic wheat straw for arsenic adsorption, J. Hazard. Mater. 193 (2011) 10–16, https://doi.org/10.1016/j.jhazmat.2011.04.093.

[13] B.K. Nath, C. Chaliha, E. Kalita, M.C. Kalita, Synthesis and characterization of ZnO:CeO_2:nanocellulose:PANI bionanocomposite. A bimodal agent for arsenic adsorption and antibacterial action, Carbohydr. Polym. 148 (2016) 397–405, https://doi.org/10.1016/j.carbpol.2016.03.091.

[14] P. González-García, Activated carbon from lignocellulosics precursors: a review of the synthesis methods, characterization techniques and applications, Renew. Sust. Energ. Rev. 82 (2018) 1393–1414, https://doi.org/10.1016/j.rser.2017.04.117.

[15] I.L.A. Ouma, E.B. Naidoo, A.E. Ofomaja, Thermodynamic, kinetic and spectroscopic investigation of arsenite adsorption mechanism on pine cone-magnetite composite, J. Environ. Chem. Eng. 6 (4) (2018) 5409–5419, https://doi.org/10.1016/j.jece.2018.08.035.

[16] L. Verma, J. Singh, Synthesis of novel biochar from waste plant litter biomass for the removal of Arsenic (III and V) from aqueous solution: a mechanism characterization, kinetics and thermodynamics, J. Environ. Manage. 248 (2019) 109235, , https://doi.org/10.1016/j.jenvman.2019.07.006.

[17] S. Rangabhashiyam, P. Balasubramanian, The potential of lignocellulosic biomass precursors for biochar production: performance, mechanism and wastewater application – a review, Ind. Crop. Prod. 128 (2019) 405–423, https://doi.org/10.1016/j.indcrop.2018.11.041.

[18] L. Hadjittofi, M. Prodromou, I. Pashalidis, Activated biochar derived from cactus fibres – Preparation, characterization and application on Cu(II) removal from aqueous solutions, Bioresour. Technol. 159 (2014) 460–464, https://doi.org/10.1016/j.biortech.2014.03.073.

[19] T. Nharingo, M. Moyo, Application of *Opuntia ficus-indica* in bioremediation of wastewaters. A critical review, J. Environ. Manage. 166 (2016) 55–72, https://doi.org/10.1016/j.jenvman.2015.10.005.

[20] U.U. Shedbalkar, V.S. Adki, J.P. Jadhav, V.A. Bapat, Opuntia and other cacti: applications and biotechnological insights, Trop. Plant Biol. 3 (2010) 136–150, https://doi.org/10.1007/s12042-010-9055-0.

[21] A. Gebrekidan, H. Nicolai, L. Vincken, M. Teferi, T. Asmelash, T. Dejenie, S. Zerabruk, K. Gebrehiwet, H. Bauer, J. Deckers, P. Luis, L. de Meester, B. van der Brugge, Pesticides removal by filtration over Cactus pear leaves: a cheap and natural method for small-scale water purification in semi-arid regions, Clean Soil Air Water 41 (3) (2013) 235–243, https://doi.org/10.1002/clen.201200042.

[22] D.I. Fox, T. Pichler, D.H. Yeh, N.A. Alcantar, Removing heavy metals in water: the interaction of Cactus mucilage and arsenate (As (V)), Environ. Sci. Technol. 46 (2012) 4553–4559, https://doi.org/10.1021/es2021999.

[23] A.A. Peláez-Cid, I. Velázquez-Ugalde, A.M. Herrera-González, J. García-Serrano, Textile dyes removal from aqueous solution using *Opuntia ficus-indica* fruit waste as adsorbent and its characterization, J. Environ. Manage. 130 (2013) 90–97, https://doi.org/10.1016/j.jenvman.2013.08.059.

[24] A.A. Peláez-Cid, M.A. Tlalpa-Galán, A.M. Herrera-González, Carbonaceous material production from vegetable residue and their use in the removal of textile dyes present in wastewater, Mater. Sci. Eng. 45 (2013) 012023https://iopscience.iop.org/article/10.1088/1757-899X/45/1/012023/pdf.

[25] M. Prodromou, I. Pashalidis, Copper(II) removal from aqueous solutions by adsorption on non-treated and chemically modified cactus fibres, Water Sci. Technol. 68 (11) (2013) 2497–2504, https://doi.org/10.2166/wst.2013.535.

[26] J.A. Fernández-López, J.M. Angosto, M.D. Avilés, Biosorption of hexavalent chromium from aqueous medium with *Opuntia* biomass, Transfus. Apher. Sci. 2014 (2014) 670249, https://doi.org/10.1155/2014/670249.

[27] L. Hadjittofi, I. Pashalidis, Uranium sorption from aqueous solutions by activated biochar fibres investigated by FTIR spectroscopy and batch experiments, J. Radioanal. Nucl. Chem. 304 (2015) 897–904, https://doi.org/10.1007/s10967-014-3868-5.

[28] X. Vecino, R. Devesa-Rey, D.M. de Lima-Stebbins, A.B. Moldes, J.M. Cruz, N.A. Alcantar, Evaluation of a cactus mucilage biocomposite to remove total arsenic from water, Environ. Technol. Inno. 6 (2016) 69–79, https://doi.org/10.1016/j.eti.2016.07.001.

[29] G. Alberti, V. Amendola, M. Pesavento, R. Biesuz, Beyond the synthesis of novel solid phases: review on modelling of sorption phenomena, Coord. Chem. Rev. 256 (2012) 28–45, https://doi.org/10.1016/j.ccr.2011.08.022.

[30] L. Largitte, R. Pasquier, A review on the kinetics adsorption models and their application to the adsorption of lead by an activated carbon, Chem. Eng. Res. Des. 109 (2016) 495–504, https://doi.org/10.1016/j.cherd.2016.02.006.

[31] S. Azizian, S. Eris, L.D. Wilson, Re-evaluation of the century-old Langmuir isotherm for modeling adsorption phenomena in solution, Chem. Phys. 513 (2018) 99–104, https://doi.org/10.1016/j.chemphys.2018.06.022.

[32] L. Sellaoui, T. Depci, A.R. Kul, S. Krani, A.B. Lamine, A new statistical physics model to interpret the binary adsorption isotherms of lead and zinc on activated carbon, J. Mol. Liq. 214 (2016) 220–230, https://doi.org/10.1016/j.molliq.2015.12.080.

[33] M.R. Gadekar, M.M. Ahammed, Modelling dye removal by adsorption onto water treatment residuals using combined response surface methodology-artificial neural network approach, J. Environ. Manage. 231 (2019) 241–248, https://doi.org/10.1016/j.jenvman.2018.10.017.

[34] F.A. Gordillo-Ruiz, F.J. Sánchez-Ruiz, D.I. Mendoza-Castillo, H.E. Reynel-Ávila, A. Bonilla-Petriciolet, Dynamic fuzzy neural network for simulating the fixed-bed adsorption of cadmium, nickel and zinc on bone char, Int. J. Environ. Sci. Technol. 15 (2018) 915–926, https://doi.org/10.1007/s13762-017-1456-2.

[35] B.G. Saucedo-Delgado, D.A. de Haro-Del Rio, L.M. González-Rodríguez, H.E. Reynel-Ávila, D.I. Mendoza-Castillo, A. Bonilla-Petriciolet, J.Rivera de la Rosa, Fluoride adsorption from aqueous solution using a protonated clinoptilolite and its modeling with artificial neural network-based equations, J. Fluorine Chem. 204 (2017) 98–106, https://doi.org/10.1016/j.jfluchem.2017.11.002.
[36] R. Tovar-Gómez, M.R. Moreno-Virgen, J.A. Dena-Aguilar, V. Hernández-Montoya, A. Bonilla-Petriciolet, M.A. Montes-Morán, Modeling of fixed-bed adsorption of fluoride on bone char using a hybrid neural network approach, Chem. Eng. J. 228 (2013) 1098–1109, https://doi.org/10.1016/j.cej.2013.05.080.
[37] D.I. Mendoza-Castillo, C.K. Rojas-Mayorga, I.P. García-Martínez, M.A. Pérez-Cruz, V. Hernández-Montoya, A. Bonilla-Petriciolet, M.A. Montes-Morán, Removal of heavy metals and arsenic from aqueous solution using textile wastes from denim industry, Int. J. Environ. Sci. Technol. 12 (2015) 1657–1668, https://doi.org/10.1007/s13762-014-0553-8.
[38] M. Gar Alalm, M. Nasr, Artificial intelligence, regression model, and cost estimation for removal of chlorothalonil pesticide by activated carbon prepared from casuarina charcoal, Sustain. Environ. Res. 28 (2018) 101–110, https://doi.org/10.1016/j.serj.2018.01.003.
[39] F. Rodriguez-Reinoso, J. Silvestre-Albero, Activated carbon and adsorption, Ref Module Mater Sci Mater Eng (2016) 1–14, https://doi.org/10.1016/B0-08-043152-6/00005-X.
[40] H. Uppal, S. Chawla, A.G. Joshi, D. Haranath, N. Vijayan, N. Singh, Facile chemical synthesis and novel application of zinc oxysulfide nanomaterial for instant and superior adsorption of arsenic from water, J. Clean. Prod. 208 (2019) 458–469, https://doi.org/10.1016/j.jclepro.2018.10.023.
[41] M. Volpe, J.L. Goldfarb, L. Fiori, Hydrothermal carbonization of *Opuntia ficus-indica* cladodes: role of process parameters on hydrochar properties, Bioresour. Technol. 247 (2018) 310–318, https://doi.org/10.1016/j.biortech.2017.09.072.
[42] H.E. Reynel-Avila, D.I. Mendoza-Castillo, A.A. Olumide, A. Bonilla Petriciolet, A survey of multi-component sorption models for the competitive removal of heavy metal ions using bush mango and flamboyant biomasses, J. Mol. Liq. 224 (2016) 1041–1054, https://doi.org/10.1016/j.molliq.2016.10.061.
[43] L.H. Velazquez-Jimenez, R.H. Hurt, J. Matos, J.R. Rangel-Mendez, Zirconium-carbon hybrid sorbent for removal of fluoride from water: oxalic acid mediated Zr (IV) assembly and adsorption mechanism, Environ. Sci. Technol. 48 (2014) 1166–1174, https://doi.org/10.1021/es403929b.
[44] S. Xin, H. Yang, Y. Chen, M. Yang, L. Chen, X. Wang, H. Chen, Chemical structure evolution of char during the pyrolysis of cellulose, J. Anal. Appl. Pyrol. 116 (2015) 263–271, https://doi.org/10.1016/j.jaap.2015.09.002.
[45] A. Mullick, S. Neogi, Acoustic cavitation induced synthesis of zirconium impregnated activated carbon for effective fluoride scavenging from water by adsorption, Ultrason. Sonochem. 45 (2018) 65–77, https://doi.org/10.1016/j.ultsonch.2018.03.002.
[46] L.K. Kian, M. Jawaid, H. Ariffin, Z. Karim, Isolation and characterization of nanocrystalline cellulose from roselle-derived microcrystalline cellulose, Int. J. Biol. Macromol. 114 (2018) 54–63, https://doi.org/10.1016/j.ijbiomac.2018.03.065.
[47] F.A. Gonçalves, H.A. Ruiz, C.C. Nogueira, E.S. dos Santos, J.A. Teixeira, G.R. de Macedo, Comparison of delignified coconuts waste and cactus for fuel-ethanol production by the simultaneous and semi-simultaneous saccharification and fermentation strategies, Fuel 131 (2014) 66–76, https://doi.org/10.1016/j.fuel.2014.04.021.
[48] D. Hong, J. Zhou, C. Hu, Q. Zhou, J. Mao, Q. Qin, Mercury removal mechanism of AC prepared by one-step activation with $ZnCl_2$, Fuel 235 (2019) 326–335, https://doi.org/10.1016/j.fuel.2018.07.103.
[49] L.D. Mafu, H.W.J.P. Neomagus, R.C. Everson, C.A. Strydom, M. Carrier, G.N. Okolo, J.R. Bunt, Chemical and structural characterization of char development during lignocellulosic biomass pyrolysis, Bioresour. Technol. 243 (2017) 941–948, https://doi.org/10.1016/j.biortech.2017.07.017.
[50] L.H. Velazquez-Jimenez, J.A. Arcibar-Orozco, J.R. Rangel-Mendez, Overview of As (V) adsorption on Zr-functionalized activated carbon for aqueous streams remediation, J. Environ. Manage. 212 (2018) 121–130, https://doi.org/10.1016/j.jenvman.2018.01.072.